JOURNAL OF COMPUTATIONAL PHYSICS 41, 34–50 (1981)

The Inversion of Autoconvolution Integrals

V. DOSE, TH. FAUSTER, AND H.-J. GOSSMANN

Physikalisches Institut der Universität Würzburg, Am Hubland, Würzburg D-8700, West-Germany

Received June 2, 1980

In this paper, we describe a procedure for inversion of autoconvolution integrals arising in several surface scientific methods. The solution is obtained by rigorous application of cubical spline functions. The method offers excellent numerical stability. Error propagation is discussed, and deconvolution examples are given for a characteristic isochromat, a soft X-ray appearance potential and an Auger electron appearance potential measurement of the iron L_{III} level.

I. INTRODUCTION

Line shapes in several surface analytical measurements are interpreted in a first approximation as the selfconvolution of the density of either occupied or empty electron states. As an example, we briefly describe appearance potential spectroscopies. In appearance potential spectroscopies, one observes electronic transitions from a core level to the unoccupied part of the conduction band of the sample produced by electron impact. Electrons with initial energy E_0 with respect to the Fermi level of the sample and with E_0 sufficient to produce a core hole are scattered to empty states above the Fermi level. The same is true for the ionized electrons. The energy excess E of an incident electron over the core level binding energy is shared with the ionized electron. Assuming energy independent transition matrix elements and neglecting core hole lifetime broadening, the rate of core hole production $P(E)$ is found to be proportional to the autoconvolution of the density of unoccupied states $N(E)$ [1]

$$P(E) \propto \int_0^E N(\varepsilon)\, N(E-\varepsilon)\, d\varepsilon. \tag{1}$$

If the core hole production is monitored by detection of characteristic X-radiation, the technique is called characteristic isochromat spectroscopy (CIS) [2]. An integral of exactly the same structure forms the basis for the interpretation of ion neutralization spectra (INS) in terms of the density of filled one electron states [3].

A different way to monitor core hole production is to measure the total X-ray flux emitted by the sample. The onset of core hole production with increasing impact energy manifests itself in a very small but abrupt increase in the total intensity of

0021-9991/81/050034–17$02.00/0

emitted X-rays. In order to suppress the slowly varying background from non-characteristic Bremsstrahlung and retrieve the signal part due to core hole production, the potential modulation differentiation technique [4] is usually applied. The observed signal is then the derivative of (1)

$$P'(E) \propto N(E) \cdot N(0) + \int_0^E N(\varepsilon)\, N'(E-\varepsilon)\, d\varepsilon. \tag{2}$$

The threshold behaviour of (2) is determined by the Fermi function and consequently, the first term in (2) vanishes. This spectroscopic technique is called soft X-ray appearance potential spectroscopy (SXAPS) and has been used extensively by Park and Houston [5]. A corresponding integral occurs in the interpretation of core–valence–valence Auger electron spectra which can be interpreted within this model in terms of the density of filled valence band states [6].

Still another method to observe core hole production is Auger electron appearance potential spectroscopy (AEAPS) [7]. In this technique, secondary electrons emitted from the sample are monitored. When the threshold for core hole production is crossed, their yield shows small increases due to Auger electron emission. In sufficiently small energy intervals, the background of all the other electrons is a quadratic function of primary beam energy. Therefore, the desired characteristic signal is retrieved by potential modulation differentiation recording the second derivative. This may be obtained from (2) by straightforward differentiation and subsequent partial integration as

$$P''(E) \propto \int_0^E N'(\varepsilon)\, N'(E-\varepsilon)\, d\varepsilon. \tag{3}$$

The aim of the present paper is to describe deconvolution methods for the three cases relying on cubical spline functions. The mathematics will be outlined in sufficient detail to enable the interested reader to solve his specific problem.

II. Deconvolution

The basic idea for inverting (1), (2), and (3) will be outlined with reference to (1) for definiteness. Details differing for the three cases will be treated in Section V. By suitable choice of reduced variables, (1) is rewritten as

$$P(y) = \int_0^y U(x)\, U(y-x)\, dx \tag{4}$$

and (2), (3) correspondingly as

$$P'(y) = \int_0^y U(x)\, U'(y-x)\, dx,$$

$$P''(y) = \int_0^y U'(x)\, U'(y-x)\, dx.$$

The threshold behaviour of the physical processes discussed translates in all three cases into $U(0) = 0$. The prominent difficulty in solving (4) for $U(y)$ is that $P(y)$ is not known as an analytical function but rather as a discrete set of experimental data $\tilde{P}_n$ which of course carry experimental uncertainty. Hagstrum and Becker [8] call an attempt to solve (4) starting with $\tilde{P}_n$ an "incorrectly posed" problem since any such attempt may lead to a catastrophic solution $U(y)$.

Before proceeding with the treatment of (4), we briefly recall the definition and prominent properties of cubical spline functions. A cubical spline function $\sigma(x)$ satisfying the boundary conditions $\sigma''(a) = \sigma''(b) = 0$ [9] provides a unique solution to the interpolation problem $\sigma(x_n) = h_n$ for $a \leqslant x \leqslant b$. $\sigma(x)$ is everywhere in (a, b), especially at the pivotal points x_n two times continuously differentiable and is a function with minimum curvature in the sense that

$$\int_a^b |h''(x)|^2\, dx \geqslant \int_a^b |\sigma''(x)|^2\, dx, \tag{5}$$

where $h(x)$ denotes any other two times differentiable solution of the interpolation problem $h(x_n) = h_n$. On each interval (x_n, x_{n+1}), $\sigma(x)$ coincides with a third order polynomial. If we drop the strong interpolation requirement $\sigma(x_n) = h_n$, an approximate interpolant may be obtained by minimizing the functional

$$\int_a^b |\sigma''(x)|^2\, dx + \lambda \sum_n (h_n - \sigma(x_n))^2 = \text{Min.} \tag{6}$$

The first term in (6) controls the requirement of minimum curvature resulting in a smooth function $\sigma(x)$, while the second term forces $\sigma(x)$ to approximate the given data set h_n. The parameter λ weights these two requirements.

Application of this scheme to the approximate solution of (4) is obvious. We simply require the minimization of the functional

$$\Phi = \int_0^{x_{\max}} |U''(x)|^2\, dx + \lambda \sum_n (P_n - \tilde{P}_n)^2, \tag{7}$$

$\tilde{P}_n$ being the experimental data while P_n is given by

$$P_n = \int_0^{y_n} U(x)\, U(y_n - x)\, dx. \tag{8}$$

To be consistent with the first term in (7), we choose $U(x)$ to be a cubical spline function. $U(x)$ is then uniquely determined by its values U_n at the pivotal points x_n, $U_n = U(x_n)$ and the boundary conditions $U''(0) = U''(x_{\max}) = 0$. The integrations in (7), (8) may then be carried out formally leading to

$$\Phi = \sum_{i,j=0}^{N} U_i W_{ij} U_j + \lambda \sum_{n=1}^{N} (P_n - \tilde{P}_n)^2, \tag{9}$$

$$P_n = \sum_{i,j=0}^{N} C_{ijn} U_i U_j, \qquad n = 1,..., N. \tag{10}$$

The calculation of matrices W_{ij} and C_{ijn} will be outlined below in Sections III, IV, and V. With these matrices given, minimization of Φ with respect to U_n leads to a system of nonlinear equations for U_n. Iterative solution of these equations will be described in Section VI.

III. Construction of Spline Functions

In order to compute the matrices W_{ij} and C_{ijn}, we need an explicit representation of $U(x)$ in terms of the unknown U_n. Due to the uniqueness of the spline interpolation problem, such a representation exists for any given set U_n. It would, however, be hopelessly complicated to evaluate this representation explicitly for the general case of arbitrarily distributed pivots x_n. For the special case of equidistant pivots, which nearly always applies to experimental conditions, the situation is more favourable, and an elegant solution to the problem can be constructed. The basic idea is that of arbitrary order Lagrangian polynomial interpolation [10]. For convenience, we put in the following $x_n = n$ and $x_{\max} = N$. Let $S(x)$ be a cubical spline function such that

$$\begin{aligned} S(i) = \delta_{i0} &= 1 \qquad \text{for} \quad i = 0 \\ &= 0 \qquad \text{for} \quad i \neq 0 \end{aligned} \tag{11}$$

with

$$S''(\pm\infty) = 0. \tag{12}$$

$S(x)$ is a symmetric function of x and can be used to construct an interpolation $U(x)$ to the set of ordinates $\{U_i\}$ by

$$U(x) = \sum_{i=0}^{N} U_i S(x - i). \tag{13}$$

$U(x)$ certainly interpolates $\{U_i\}$ but does not yet satisfy the boundary conditions

$$U''(0) = U''(N) = 0. \tag{14}$$

It rather satisfies

$$U''(\pm\infty) = 0. \tag{15}$$

Boundary conditions (14) may be met by a simple modification of (13). We define two additional ordinates U_{-1} and U_{N+1} at $x = -1$ and $x = N + 1$, respectively, and replace (13) by

$$U(x) = \sum_{i=-1}^{N+1} U_i S(x - i). \tag{16}$$

$U(x)$ still interpolates $\{U_i\}$ for arbitrary U_{-1} and U_{N+1} in the range $0 \leqslant x \leqslant N$. We may therefore choose U_{-1} and U_{N+1} such that (14) is fulfilled. This leads to

$$U_{-1} = \frac{F_0 S''(1) - F_N S''(N+1)}{S''(1)^2 - S''(N+1)^2}, \tag{17}$$

$$U_{N+1} = \frac{F_N S''(1) - F_0 S''(N+1)}{S''(1)^2 - S''(N+1)^2}, \tag{18}$$

where

$$F_0 = -\sum_{i=0}^{N} S''(i)\, U_i, \qquad F_N = -\sum_{i=0}^{N} S''(N-i)\, U_i. \tag{19}$$

Equations (16) through (19) represent the desired explicit spline representation of $U(x)$ in terms of arbitrary unknown $\{U_i\}$ for $0 \leqslant x \leqslant N$. It remains to evaluate the function $S(x)$ satisfying (11). With the abbreviations

$$S(x) = S_i(x - i), \qquad i \leqslant x \leqslant i + 1, \tag{20}$$

and taking $x - i = z$, we have for $S_i(z)$, $0 \leqslant z \leqslant 1$,

$$S_i(z) = a_i z^3 + b_i z^2 + c_i z + d_i. \tag{21}$$

Applying the conditions of continuity of S, S' and S'' at the pivotal points yields the explicit expressions

$$S_0(z) = (3\sqrt{3} - 4)\, z^3 + 3(1 - \sqrt{3})\, z^2 + 1, \tag{22}$$

$$S_1(z) = 3[(5 - 3\sqrt{3})\, z^3 + (2\sqrt{3} - 3)\, z^2 + (\sqrt{3} - 2)z], \tag{23}$$

$$S_{i+1}(z) = \alpha S_i(z), \qquad \alpha = \sqrt{3} - 2, \qquad i \geqslant 1. \tag{24}$$

Since $S(x)$ is a symmetric function of x, it follows that

$$S_i(z) = S_{-i-1}(1 - z). \tag{25}$$

A graph of the function $S(x)$ is displayed for illustration purposes in Fig. 1.

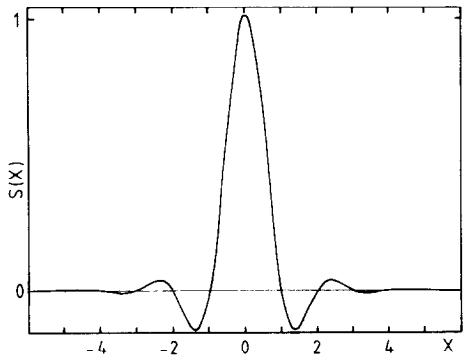

FIG. 1. $S(x)$ is the cubical spline function solving the interpolation problem $S(i) = \delta_{i,0}$.

IV. EVALUATION OF MATRIX W

From (7) and (9), the matrix W is defined by

$$\int_0^N |U''(x)|^2 \, dx = \sum_{i,j=0}^{N} U_i W_{ij} U_j. \tag{26}$$

Obviously, W is symmetric. Integrating (26) two times by parts and using the fact that the fourth derivative of U is zero on each interval $(n, n+1)$, we get

$$\int_0^N |U''(x)|^2 \, dx = \sum_{i=0}^{N-1} (U_i U'''(i^+) - U_{i+1} U'''((i+1)^-)). \tag{27}$$

The superscripts "+" and "−" denote the left- and right-hand limits, respectively. Using the explicit representation of $U(x)$ as given in (16) and (20), (27) may be written as

$$\sum_{i,j=0}^{N} U_i W_{ij} U_j = \sum_{i=0}^{N-1} \sum_{j=-1}^{N+1} (U_i U_j S'''_{i-j} - U_{i+1} U_j S'''_{i-j}). \tag{28}$$

We have now suppressed the "+" and "−" superscripts because the third derivative of S is constant on each interval. After insertion of numerical values for S''' from (22) through (25) and for U_{-1} and U_{N+1} from (17) and (18), comparison of coefficients of products $U_i U_j$ on both sides of (28) would yield the matrix elements W_{ij}. They would, however, depend on N. This is inconvenient and, in fact, unnecessary if

consideration of numerical accuracy is taken into account. Since $\alpha^{16} \sim 7 \cdot 10^{-10}$, we can approximate α^n by zero for $n > 16$ and rewrite (17) through (19):

$$U_{-1} = (1 + 1/\sqrt{3})\, U_0 - \sum_{i=1}^{N} \alpha^{i-1} U_i, \tag{29}$$

$$U_{N+1} = (1 + 1/\sqrt{3})\, U_N - \sum_{i=1}^{N} \alpha^{i-1} U_{N-i}. \tag{30}$$

With these approximations, the evaluation of (28) leads to matrix elements W_{ij} which are now independent of N. They are listed in (31),

$$W_{00} = 6(2 - \sqrt{3}),$$

$$W_{01} = 6(6\sqrt{3} - 11),$$

$$W_{0i} = 36(7 - 4\sqrt{3})\, \alpha^{i-2}, \qquad i \geqslant 2.$$

For $i \geqslant 1, j \geqslant 1$ and $i + j \leqslant N$,

$$W_{ii} = 12(3\sqrt{3} - 4) - 36(7\sqrt{3} - 12)\, \alpha^{2i-2},$$

$$W_{i,i+1} = 6(19 - 12\sqrt{3}) - 36(7\sqrt{3} - 12)\, \alpha^{2i-1}$$

and for $|i - j| \geqslant 2$,

$$W_{ij} = 36(7\sqrt{3} - 12)(\alpha^{|i-j|-2} - \alpha^{i+j-2}). \tag{31}$$

They obey the symmetry relations

$$W_{ij} = W_{ji} = W_{N-i,N-j} = W_{N-j,N-i}. \tag{32}$$

V. Evaluation of Matrix C

Contrary to W, the matrix C is different for each of the three cases in (4). We present only the first one in some detail. For the other two cases, we give only the relevant results.

Equating (8) and (10), and using representation (16) for $U(x)$, we obtain

$$\sum_{i,j=0}^{N} C_{ijn} U_i U_j = \sum_{i,j=-1}^{N+1} U_i U_j \int_0^n S(x - i)\, S(n - x - j)\, dx. \tag{33}$$

Let us denote the integral by

$$h_{ijn} = \int_0^n S(x - i)\, S(n - x - j)\, dx; \tag{34}$$

then the following symmetry relations can be verified easily:

$$h_{ijn} = h_{jin} = h_{n-i,n-j,n} = h_{n-j,n-i,n}. \tag{35}$$

The relation between C_{ijn} and h_{ijn} can be worked out by using approximations (29) and (30), and equating coefficients of $U_i U_j$ on both sides of (33).

With

$$a_0 = 1 + 1/\sqrt{3}; \qquad a_i = -\alpha^{i-1}, \quad i \geqslant 1, \tag{36}$$

we obtain

$$\begin{aligned} C_{ijn} = {} & h_{ijn} + a_i h_{-1,j,n} + a_j h_{i,-1,n} + a_{N-i} h_{N+1,j,n} + a_{N-j} h_{i,N+1,n} \\ & + a_i a_j h_{-1,-1,n} + a_i a_{N-j} h_{-1,N+1,n} + a_{N-i} a_j h_{N+1,-1,n} \\ & + a_{N-i} a_{N-j} h_{N+1,N+1,n}. \end{aligned} \tag{37}$$

The problem is now reduced to the evaluation of the integrals h_{ijn}. To do this, we

TABLE I

i	j	i+j-n	h_{ijn} / q
i < 0	j < 0		nB
	j = 0		(n-1)B + C
	0<j<n		$(n-j-1)B+C+D+[1-\alpha^{2(j-1)}]E$
	j = n		$D+[1-\alpha^{2(n-1)}]E$
	j > n		$[1-\alpha^{2n}]E\,\alpha^{2(j-n-1)}$
i = 0	j = 0	< -1	(n-2)B + 2C
		= -1	A
	0<j<n	< -1	$(n-j-2)B+2C+D+[1-\alpha^{2(j-1)}]E$
		= -1	$A+D+[1-\alpha^{2(j-1)}]E$
	j = n	= 0	$F_1+[1-\alpha^{2(n-1)}]E$
	j > n	= 1	$D+[1-\alpha^{2(n-1)}]E$
		> 1	$D+[1-\alpha^{2(n-1)}]E$
0<i<n	0<j<n	< -1	$(n-i-j-2)B+2C+2D+[2-\alpha^{2(i-1)}-\alpha^{2(j-1)}]E$
		= -1	$A+2D+[1-\alpha^{2(i-1)}+1-\alpha^{2(n-i-2)}]E$
		= 0	$F_1+F_2+[2-\alpha^{2(i-1)}-\alpha^{2(j-1)}]E$
		= 1	$A+2D+[2-\alpha^{2(n-i-1)}-\alpha^{2(i-2)}]E$
		> 1	$(i+j-n-2)B+2C+2D+[2-\alpha^{2(n-i-1)}-\alpha^{2(n-j-1)}]E$
	j = n	= 1	$A+D+[1-\alpha^{2(n-i-1)}]E$
		> 1	$(i-2)B+2C+D+[1-\alpha^{2(n-i-1)}]E$
	j > n	> 1	$(i-1)B+C+D+[1-\alpha^{2(n-i-1)}]E$
i = n	j = 0	= 0	$F_2+[1-\alpha^{2(n-1)}]E$
	j = n	= 1	A
		> 1	(n-2)B + 2C
	j > n	> 1	(n-1)B + C
i > n	j > n		nB

split the integration interval $(0, n)$ in n subintervals of length 1. Suitable choice of the integration variables then yields with definition (20) for $S(x)$

$$h_{ijn} = \sum_{K=0}^{n-1} \int_0^1 S_{K-i}(x)\, S_{n-j-K-1}(1-x)\, dx. \tag{38}$$

The symmetry and recurrence relations (24) and (25) simplify the calculation even further. It can be shown that there are only six different integrals in (38) which have to be calculated explicitly.

Table I finally lists the coefficients h_{ijn}, divided by a factor $\alpha^{|i+j-n|}$. Not shown are the h_{ijn} for $i > j$ since they can be obtained by use of (35). The constants A through F_2 are given in the first column of Table II.

For the first derivative of autoconvolution integrals, the coefficients h_{ijn} are defined by

$$h_{ijn} = \int_0^n S(x-i)\, S'(n-x-j)\, dx \tag{39}$$

with the symmetry relations

$$h_{ijn} = h_{jin} = -h_{n-i,n-j,n} = -h_{n-j,n-i,n}, \tag{40}$$

except if $i = 0$ and $j = n$ where $h_{0,n,n} = -h_{n,0,n}$.

The relation (37) between the matrix elements C_{ijn} and the coefficients h_{ijn} holds

TABLE II

	0th Derivative	1st Derivative	2nd Derivative
A	$-\frac{1}{140}(9\sqrt{3}+98)$	$\frac{13}{20}(\sqrt{3}+2)$	$-\frac{3}{10}(5\sqrt{3}+4)$
B	$-\frac{3}{7}$	$\frac{3}{10}\sqrt{3}$	$\frac{18}{5}$
C	$-\frac{1}{70}(39+2\sqrt{3})$	$\frac{3}{20}(3\sqrt{3}+4)$	$\frac{3}{10}(5-2\sqrt{3})$
D	$\frac{1}{14}(15-7\sqrt{3})$	$\frac{3}{20}(4-\sqrt{3})$	$\frac{3}{10}(16\sqrt{3}-29)$
E	$\frac{1}{140}(77\sqrt{3}-132)$	0	$\frac{9}{10}(12-7\sqrt{3})$
F_1	$\frac{1}{70}(94-37\sqrt{3})$	$\frac{1}{2}$	$\frac{21}{5}(\sqrt{3}-2)$
F_2	F_1	$-F_1$	F_1
q:			
$i+j-n>0$	$\alpha^{\lvert i+j-n\rvert}$	$-\alpha^{\lvert i+j-n\rvert}$	$\alpha^{\lvert i+j-n\rvert}$
$i+j-n\leqq 0$	$\alpha^{\lvert i+j-n\rvert}$	$\alpha^{\lvert i+j-n\rvert}$	$\alpha^{\lvert i+j-n\rvert}$

also in this case. The resulting h_{ijn} are formally identical with the previous case and can again be obtained from Table I. The constants A through F_2 are different of course; they are listed in the second column of Table II.

For the last case of (4), the coefficients h_{ijn} are determined by

$$h_{ijn} = \int_0^n S'(x-i)\, S'(n-x-j)\, dx. \tag{41}$$

The symmetry relations analogous to (35) are

$$h_{ijn} = h_{jin} = h_{n-i,n-j,n} = h_{n-j,n-i,n}. \tag{42}$$

Equation (37) is correct also for this case. The coefficients h_{ijn} can again be obtained from Table I with the values of the constants A through F_2 given in the last column of Table II.

VI. Iterative Solution of the Nonlinear Equations

As already pointed out in Section II, the solution of the deconvolution problem results from minimization of the functional

$$\Phi = \sum_{i,j=1}^{N} U_i W_{ij} U_j + \lambda \sum_{n=1}^{N} (P_n - \tilde{P}_n)^2 \tag{43}$$

with

$$P_n = \sum_{i,j=1}^{N} C_{ijn} U_i U_j, \tag{44}$$

where we have used explicitly the initial condition $U_0 = 0$. The necessary conditions for the minimum of functional (43) are

$$\frac{\partial \Phi}{\partial U_K} = 2 \sum_{i=1}^{N} W_{Ki} U_i + 2\lambda \sum_{n=1}^{N} (P_n - \tilde{P}_n) \frac{\partial P_n}{\partial U_K} = 0, \qquad K = 1,..., N, \tag{45}$$

where we have used the symmetry of matrix W, Eq. (32). This system of nonlinear equations can be linearized, and we arrive at the following equations for the corrections $\Delta U_K^{(m)}$ in the mth iteration step:

$$U_K^{(m+1)} = U_K^{(m)} + \Delta U_K^{(m)}, \tag{46}$$

$$\sum_{j=1}^{N} (W_{Kj} + 4\lambda \sum_{i=1}^{N} G_{iK}^{(m)} G_{ij}^{(m)} + 2\lambda V_{Kj}^{(m)})\, \Delta U_j^{(m)}$$

$$= 2\lambda \sum_{j=1}^{N} G_{jK}^{(m)} \tilde{P}_j - \sum_{j=1}^{N} (W_{Kj} + 2\lambda \sum_{i=1}^{N} G_{iK}^{(m)} G_{ij}^{(m)})\, U_j^{(m)}. \tag{47}$$

The matrices $G^{(m)}$ and $V^{(m)}$ are defined by

$$G_{Ki}^{(m)} = \sum_{j=1}^{N} C_{ijK} U_j^{(m)}, \tag{48}$$

$$V_{ij}^{(m)} = \sum_{K=1}^{N} C_{ijK} \left(\sum_{l=1}^{N} G_{Kl}^{(m)} U_l^{(m)} - \tilde{P}_K \right). \tag{49}$$

In deriving (47), we have used the relation

$$C_{ijK} = C_{jiK} \tag{50}$$

which can be verified in all three cases from Eqs. (35), (37), (40), and (42).

The iteration process can be terminated if $\Delta U_K^{(m)}$ is sufficiently small compared with $U_K^{(m)}$. Of course, the $U_K^{(m)}$ depend on the parameter λ which determines the smoothness of the solution. A proper choice of λ is such that the differences $|P_n - \tilde{P}_n|$ are of the same order as the estimated or measured experimental uncertainty of the $\tilde{P}_n$. This value of λ must be determined by repeated trial and error computations. Because of the errors $\sigma_{\tilde{P}_j}$ in the experimental data $\tilde{P}_j$, the calculated values of U_i are also erroneous. As in [11], their errors σ_{U_i} can be obtained by adding "noise" to the input data $\tilde{P}_n$ and calculating the corresponding U_i. A more rigorous way is to use the general error propagation law

$$\sigma_{U_i}^2 = \sum_{j=1}^{N} \left| \frac{\partial U_i}{\partial \tilde{P}_j} \right|^2 \sigma_{\tilde{P}_j}^2. \tag{51}$$

The partial derivatives can be obtained by rewriting (45) for $\tilde{P}_n + \Delta \tilde{P}_n$ and the corresponding $U_i + \Delta U_i$. Keeping only linear terms in ΔU_i and $\Delta \tilde{P}_n$ and using (45) for U_i and $\tilde{P}_n$, we arrive at the following relation between ΔU_i and $\Delta \tilde{P}_j$:

$$\sum_{j=1}^{N} \left(W_{Kj} + 4\lambda \sum_{i=1}^{N} G_{iK} G_{ij} + 2\lambda V_{Kj} \right) \Delta U_j = 2\lambda \sum_{j=1}^{N} G_{jK} \Delta \tilde{P}_j. \tag{52}$$

Defining a matrix R by

$$R_{Kj} = W_{Kj} + 4\lambda \sum_{i=1}^{N} G_{iK} G_{ij} + 2\lambda V_{Kj} \tag{53}$$

and assuming that the inverse matrix R^{-1} of R exists, we obtain for the partial derivatives

$$\frac{\partial U_i}{\partial \tilde{P}_j} = 2\lambda \sum_{K=1}^{N} (R^{-1})_{iK} G_{jK}. \tag{54}$$

VII. Practical Aspects of Programming the Algorithm

In the preceding sections, we have presented the mathematics of our method for the inversion of autoconvolution integrals. However, there are still some points to consider in programming this algorithm on a digital computer. In deriving the matrices W_{ij} and C_{ijK}, we have already assumed that we can neglect powers of α^n for $n > 16$. If we apply this approximation systematically in computing the coefficients h_{ijn}, most of them are zero, and the sum (37) reduces to a few terms for most of the combinations of i, j and n. Since the calculation of the matrices G and V is rather time consuming, it is necessary to have a good initial guess for $U_i^{(1)}$ in order to reduce the number of iteration steps. We use for the calculation of $U_i^{(1)}$ a modified version of the algorithm described in [12].

In the evaluation of the errors σ_{U_i}, it is necessary to have a solution U_i with sufficiently high accuracy since we have assumed in deriving (52) that Eq. (45) is fulfilled exactly.

VIII. Application to Appearance Potential Spectra

The deconvolution method described in the previous sections has been employed to process a CIS measurement by Hanzely and Liefeld [13], as well as SXAPS and AEAPS measurements performed in our laboratory. The three types of experiments correspond to deconvolution of Eqs. (1) through (3), respectively, and should yield essentially identical results. Deviations of the solutions from each other may be attributed to different experimental resolutions. Figure 2a shows the CIS measurement, the corresponding deconvolution being displayed in Fig. 2b. This result was obtained with a value of 300 for λ, the input data having been scaled to $\sum_{n=1}^{N} \tilde{P}_n^2 = 1$. The lower part of Fig. 2a shows the difference between the experimental data and the autoconvolution of the result in Fig. 2b magnified by an appropriate factor. The two dashed horizontal lines indicate the confidence limits due to experimental uncertainty. The resulting errors in the deconvolution result have been calculated with (51) through (54) and are displayed as error bars in Fig. 2b. These mean deviations are of the same order as those estimated by varying the input data according to [11]. A variation in the solution of the same size is obtained by changing the parameter λ from 30 to 3000. Corresponding calculations have been carried out for SXAPS and AEAPS spectra of the iron L_{III} line; the results are displayed in Figs. 3 and 4.

A comparison of the three deconvolution results is given in Fig. 5. We consider the agreement between the three cases as excellent regarding the differences in the experimental approach.

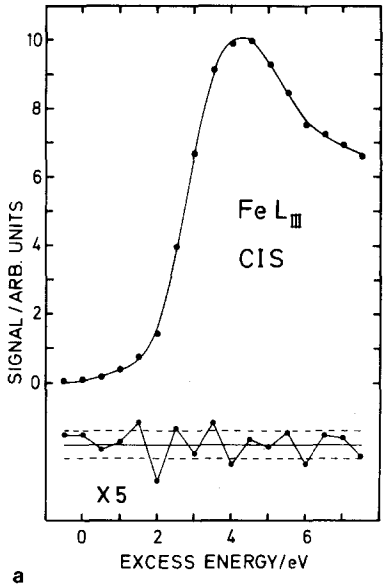

FIG. 2. (a) The dots represent a CIS measurement of an iron L_{III}-line from [13], whereas the solid line gives the autoconvolution of the deconvolution result in (b). In the lower part, differences between autoconvolution and data points (magnified by 5) are compared with the experimental error (dashed lines). (b) Deconvolution result of (a), $\lambda = 300$, with calculated error bars.

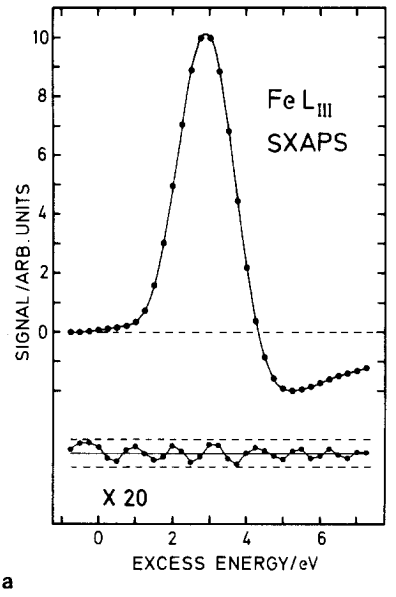

FIG. 3. (a) The dots represent a SXAPS measurement of an iron L_{III}-line. The solid line gives the autoconvolution of the deconvolution result in (b). In the lower part, differences between autoconvolution and data points (magnified by 20) are compared with the experimental error (dashed lines). (b) Deconvolution result of (a), $\lambda = 300$, with calculated error bars.

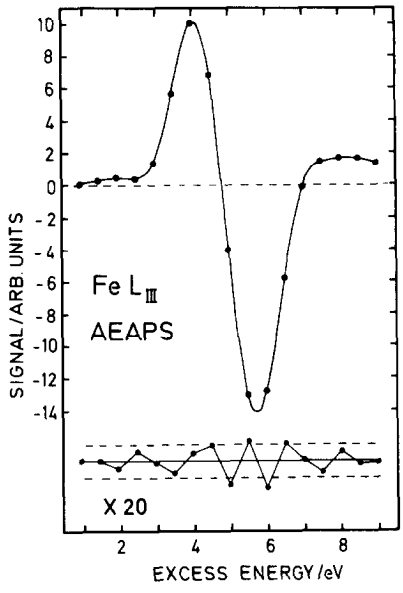

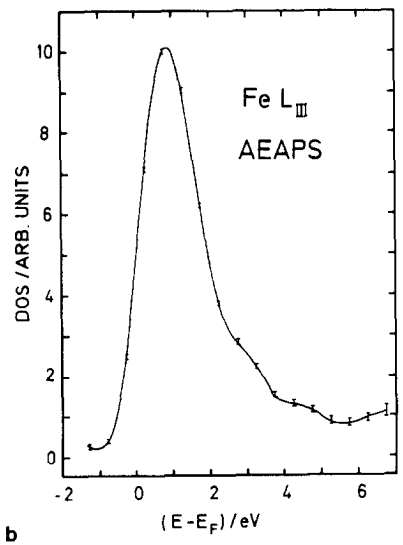

FIG. 4. (a) The dots represent an AEAPS measurement of an iron L_{III}-line. The solid line gives the autoconvolution of the deconvolution result in (b). In the lower part, differences between autoconvolution and data points (magnified by 20) are compared with the experimental error (dashed lines). (b) Deconvolution result of (a), $\lambda = 300$, with calculated error bars.

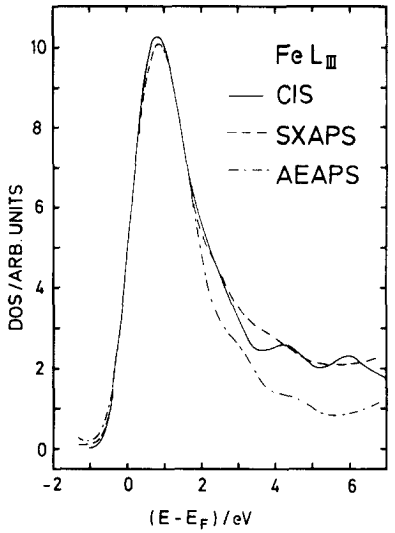

FIG. 5. Comparison of deconvolution results of iron L_{III}-measurements.

IX. DISCUSSION

There have been several other approaches to the problem treated in this paper. A critical review of early work including the Fourier transform technique was given by Hagstrum and Becker [8]. They developed a sequential deconvolution procedure applicable to cases where the unfold $U(x)$ exhibits a step-like behaviour at the origin $x = 0$. Data smoothing preceding the deconvolution is necessary in their method. The problem of data smoothing arises necessarily in all other solutions known so far. Thus, the approach by Martinez [14] differs from the earlier work of Mularie and Peria [15] only as far as smoothing of both data and Fourier transforms are concerned. Onsgaard and Morgan [16] and Garot and Boiziau [17] present solutions in terms of spline functions. In both cases, a trial autoconvolution is fitted to the experimental input data by least-squares techniques. Usually at least twice as many points in the input data as for the unfold are required in order to get the necessary degrees of freedom in the fitting procedure. Our method, however, offers complete transfer of information. The number of data points equals the number of ordinates of the calculated unfold. The treatment of noise is incorporated in the algorithm in a somehow natural and mathematically consistent manner. The accuracy of the unfold can always be matched to the precision of the input data by suitable choice of the Lagrange parameter λ.

REFERENCES

1. R. L. PARK AND J. E. HOUSTON, *J. Vac. Sci. Technol.* **10** (1973), 176.
2. R. J. LIEFELD, *in* "Soft X-Ray Band Spectra," (D. J. Fabian, Ed.), p. 133, Academic Press, New York, 1968.
3. H. D. HAGSTRUM, *J. Vac. Sci. Technol.* **12** (1975), 7.
4. J. E. HOUSTON AND R. L. PARK, *Rev. Sci. Instrum.* **43** (1972), 1437.
5. R. L. PARK AND J. E. HOUSTON, *J. Vac. Sci. Technol.* **11** (1974), 1.
6. R. WEISSMANN, W. SCHNELLHAMMER, R. KOSCHATZKY, AND K. MÜLLER, *Appl. Phys.* **14** (1977), 283.
7. M. L. DEN BOER, P. I. COHEN, AND R. L. PARK, *Surface Sci.* **70** (1978), 643.
8. H. D. HAGSTRUM AND G. E. BECKER, *Phys. Rev. B* **4** (1971), 4187.
9. J. STOER, "Einführung in die Numerische Mathematik," Vol. I, p. 76, Springer, Berlin/Heidelberg/New York, 1972. These are the only boundary conditions without knowledge about the function to be interpolated.
10. M. ABRAMOWITZ AND I. A. STEGUN, "Handbook of Mathematical Functions," p. 878, Dover, New York, 1965.
11. V. DOSE AND TH. FAUSTER, *Appl. Phys.* **20** (1979), 299.
12. V. DOSE AND H. SCHEIDT, *Appl. Phys.* **19** (1979), 19.
13. S. HANZELY AND R. J. LIEFELD, *in* "Electron Density of States," p. 319, NBS Special Publication 323, Washington, D.C., 1971.
14. V. MARTINEZ, *J. Elec. Spec.* **17** (1979), 33.
15. W. M. MULARIE AND W. T. PERIA, *Surface Sci.* **26** (1971), 125.
16. J. H. ONSGAARD AND P. MORGAN, *J. Vac. Sci. Technol.* **15** (1978), 44.
17. C. GAROT AND C. BOIZIAU, *Le Vide* **96** (1979), 17.